UCRL- 94115
PREPRINT

TIBER II--AN UPGRADED TOKAMAK IGNITION/BURN EXPERIMENTAL REACTOR

C. D. Henning. B. G. Logan, L. J. Perkins, W. L. Barr,
R. H. Bulmer, R. S. Devoto, J. N. Doggett, M. Fenstermacher,
B. M. Johnston J. D. Lee, G. Listvinski, J. R. Miller,
W. S. Neef, M. Sawan, D. S. Slack, L. Summers, and C. E. Wagner

This Paper Was Prepared For Submittal To The
7th Topical Meeting on the Technology of
Fusion Energy, MGM Grand Hotel, Reno, NV;
American Nuclear Society; June 15-19, 1986

June 5, 1986

TIBER II--AN UPGRADED TOKAMAK IGNITION/BURN EXPERIMENTAL REACTOR

C. D. Henning, B. G. Logan,
L. J. Perkins, W. L. Barr,
R. H. Bulmer, R. S. Devoto,
J. N. Doggett, B. M. Johnston,
J. D. Lee, J. R. Miller,
W. S. Neef, D. S. Slack,
and L. Summers
Lawrence Livermore National Laboratory,
University of California
Livermore, CA 94550
(415)422-0235

M. Fenstermacher, G. Listvinski,
and C. E. Wagner
TRW Corporation
Redondo Beach, CA 90278
(415)423-6308

M. Sawan
University of Wisconsin--Madison
Madison, WI 53706
(608) 263-5093

ABSTRACT

We are designing a minimum-size Tokamak Ignition/Burn Reactor (TIBER II). This design incorporates physics requirements, neutron wall loading and fluence parameters that will make it compatible with a nuclear testing mission. Reactor relevant physics will be tested by using current drive and steady-state operation. Although the design accommodates several current drive options, including neutral beams, the base case uses a combination of lower hybrid and electron-cyclotron radio frequency power. Minimum neutron shielding, compact structures, high magnet-current densities, and remotely maintainable vacuum seals, all contribute to the compact size.

INTRODUCTION

In an earlier design of the Tokamak Ignition/Burn Experimental Research Reactor (TIBER),[1] we illustrated how compact, steady-state reactors of low cost could demonstrate pulsed ignition and sustained fusion burn. To reduce the size and cost of the tokamak, we made the following aggressive design assumptions. Neutron shielding was minimized by radiation hardening of the magnets to achieve the desired small device size. In addition, a high-field plasma-shaping coil was used in the usual ohmic-heating coil position. By shaping the plasma profile with the coil, we achieved a higher plasma beta in the first stability regime. In this compact design, limited volt·seconds in the poloidal field coils are augmented by steady-state current drive.

We upgraded the TIBER concept to TIBER II, in which the more conservative Kaye-Goldston confinement scaling is assumed in concert with recent tokamak fusion test reactor (TFTR) and JET results. Also, a double-poloidal divertor is added to control impurities as in Joint European Torus (JET), and further current-drive options are considered, including electron-cyclotron heating (ECH), lower-hybrid (LH) resonant heating, and negative-ion beams. These revisions have caused the major radius of the tokamak to grow from 2.6 to 3.0 meters. A crescent plasma shape ($\kappa = 2.2$, $\delta = 0.58$) leads to a critical beta of 8%, with a plasma current of 10 MA.

PLASMA PHYSICS

Physics parameters for the two operating modes of TIBER II and the corresponding parameters from the earlier TIBER design are listed in Table 1. As in the previous study, these parameters describe steady-state burn-operating points for which the plasma current is sustained noninductively. The baseline parameters represent TIBER-II performance under conservative assumptions in confinement scaling, safety factors, and beta and density limits. The high-performance case shows the improvements that might be achieved if sawteeth activity and disruptions can be controlled with "smart heating," allowing operation at higher plasma current, lower safety factors, and less conservative beta-limit assumptions.

The baseline case produces 277 MW of fusion power at a plasma current of 10 MA. This gives an average neutron wall loading over the first wall of 1.2 MW/m^2. The peak wall loading $\hat{\Gamma}$ occurs on the outside of the torus at the equatorial plane. Calculations have shown that, for TIBER II, the peak wall flux is about 1.5 times higher, or $\hat{\Gamma} = 1.8$ MW/m^2. Plasma current is sustained in steady state by a combination of LH and electron-cyclotron resonance (ECR) current drive. The total external current-drive power absorbed is $P_{rf} = 53.4$ MW ($P_{LH} = 20$ MW, $P_{ECR} = 33.4$ MW),

Table 1. TIBER-II plasma parameters.

Parameter	TIBER	TIBER II Baseline	TIBER II High performance
P_F (MW)	200	277	361
P_{sync} (MW)	0	5.7	13.2
P_{rf} (MW)	40	53.4	53.9
Q	5	5.2	6.7
I_p (MA)	7.4	10	15
$\langle T_e \rangle$ (keV)	24	24.6	35.2
$\langle n_e \rangle$ ($10^{20} m^{-3}$)	0.94	1.18	1.11
$\langle \beta \rangle$ (%)	8.1	6	9.2
q (0)	1.0	1.0	0.67
q (a)	3.2	3.91	1.68
R (m)	2.6	3.0	3.0
a (m)	0.72	0.83	0.81
κ	1.94	2.2	2.2
δ	0.60	0.58	0.26
$\langle \Gamma_{wall} \rangle$ (MW/m^2)	1.0	1.2	1.6
$\hat{\Gamma}_{wall}$ (MW/m^2)	1.5	1.8	2.4

giving a physics Q = 5.2. We also assume that this power is eventually deposited as heat in the electron energy balance. For ECR current drive, the efficiency is

$$\eta_{ECR} = 0.45 \frac{\langle Te \rangle \text{ (keV)}}{R(m)\ \langle n_{e20} \rangle\ (m^{-3})\ \ln\Lambda} \text{ A/W} ,$$

where the plasma density $\langle n_{e20} \rangle = \langle n_e \rangle / 1.0 \times 10^{20}$. The coefficient (0.45) is consistent with the nonrelativistic analysis of Karney and Fisch[2] for the baseline TIBER-II plasma. An average optical thickness for first harmonic ordinary-mode ECR waves [launched from the outside (low-field side) of the torus and absorbed on the high-field side of the minor axis] is about 400. The baseline efficiency of ECR current drive η_{ECR} is 0.17 A/W with a $\ln\Lambda$ of 17.9. Conservative Kaye-Goldston scaling is assumed with a moderate H-mode enhancement factor (given the double-null poloidal divertors in TIBER II) of 1.3. Thermal diffusivities of electrons and ions are taken to be equal in accordance with the Ignition Physics Study Group (for the Office of Fusion Energy Compact Ignition Tokamak) recommendations. In addition, we conservatively assume that both the alpha power P_α and P_{rf} degrade confinement according to the Kaye-Goldston scaling law. Finally, to limit the potential for disruptions, the operating beta is taken to be 75% of the magnetohydrodynamic (MHD) critical beta limit. A safety factor on the plasma edge of q(a) = 3.9 further reduces risk of disruptions. The value on axis q(0) = 1.0 reduces sawteeth activity. The average plasma density is

$$\langle n_e \rangle = 1.18 \times 10^{20}\ m^{-3} ,$$

well below the Murakami density limit

$$n_{max} = 3.4 \times 10^{20} .$$

Comparing the TIBER II baseline to TIBER shows an increase in fusion power resulting from the increase in plasma size and density. The energy multiplication Q remains nearly the same since the required current drive power is higher in the new device. This results partly from the increase in plasma volume and partly from more conservative energy confinement scaling assumed in TIBER II. Finally, the operating beta is lower due to the conservative assumption that

$$\beta_{op} = 0.75 \times \beta_{crit} .$$

A high-performance case represents possible TIBER II parameters if "smart heating" can be achieved to suppress sawteeth activity in the plasma core when q(0) < 1 and to control the edge plasma conditions at low q(a) to limit disruptions. The benefits are better energy confinement from the higher plasma current, higher fusion power (P_F = 361 MW compared with 277 MW), and wall loading ($\langle \Gamma \rangle$ = 1.6, $\hat{\Gamma}$ = 2.4 MW/m^2 compared with 1.2 and 1.8 MW/m^2), using the same current drive power. This results in a plasma Q = 6.7.

COMPACT DIVERTOR

TIBER's edge plasma and compact divertor operate in a high recycling mode. This generates the high density needed to allow the edge plasma to shield the core plasma from the gas and impurities generated at the divertor plates. It also allows the charged particle power to be carried out by a high flux of low-energy particles in order to reduce the sputter-erosion of the plates.

Figure 1 shows the toroidally symmetrical divertor with its vented plates and vacuum duct. Identical divertors are located at the top and bottom of the machine to provide the surface area of the plates needed to keep the average heat load below about 2 MW/m^2. The

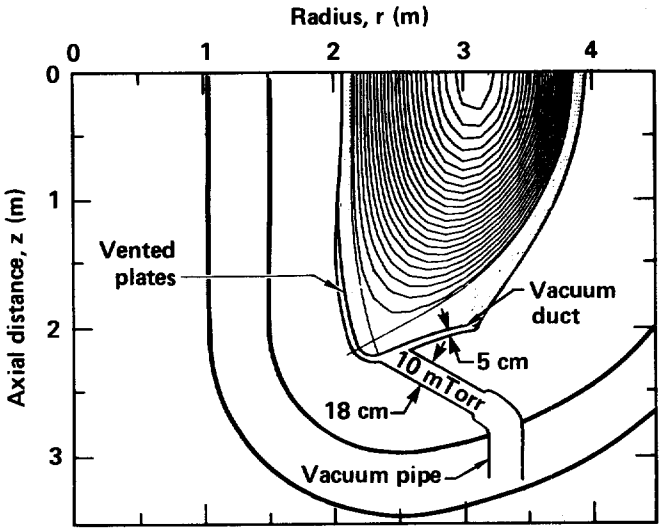

Figure 1. The compact divertor concept for TIBER II. A dense, cool edge plasma is produced by the high recycle rate. Gas is removed through the many venting ports in the divertor plates. Pressure in the duct is 10 mTorr.

vented-plate concept allows the designer some choice in the operating gas pressure in the duct and in the recycle fraction. This plate also allows the vacuum duct to be thin so that it displaces only a small amount of neutron shielding. A thin duct has the additional advantage of allowing the close placement of coils to produce the ergodic edge magnetic field that might be needed to distribute the heat during off-normal operation.

Particle and Power Fluxes in the Edge Plasma

The edge plasma shown in Fig. 1 has a thickness in the midplane equal to about five radial diffusion lengths. The thickness scales inversely as the magnetic field, giving the outer edge plasma a thickness that is nearly twice that of the inner one. To reduce the bombardment of the first wall by ions, the inner and outer walls are located on magnetic-flux surfaces. Only the divertor plates are allowed to cross field lines and intercept edge-plasma particles.

To model the particle and power flow in the edge plasma, consider a helical tube of magnetic flux extending from the upper to the lower divertor; then map the field lines in this tube into straight lines, as shown in Fig. 2. Because of symmetry, only half of the tube needs to be considered. The flux tube shown in Fig. 2 has a length L that is one-quarter of the length that would bring a field line back to the same poloidal location: $L = \pi R_0 q_a/2 = 18.3$ m. Different scales are used in

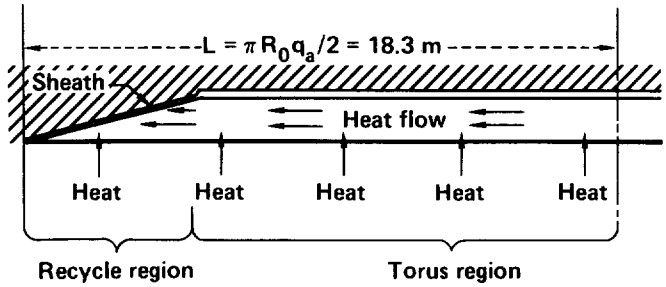

Figure 2. Model for calculating the particle and power flow in the edge plasma. Heat is absorbed uniformly along the length, and flows along magnetic field lines to the divertor plate at the left-hand side of the figure. Gas recycling occurs only near the divertor plates.

the figure for vertical and horizontal distances because the length is so much greater than the thickness, which varies slightly with poloidal location, but is roughly 0.1 m.

Heat is absorbed uniformly all along the length of the flux tube because of radial conduction from the core plasma. We refer to the region where the edge plasma flows parallel to the first wall as the "torus region," and to the region where it flows in front of the divertor plates and interacts with gas as the "recycle region."

In the torus region, little gas ionization takes place, and the small particle flux that is due to the steady loss of hot ions from the core is ignored. Heat is transported only by classical electron thermal conduction along the field lines in this region of the edge plasma:

$$Q = -\kappa T^{5/2}(dT/ds) = \int_0^s P_1 ds = P_1 s \quad ,$$

where Q (W/m^2) is the heat flux, $\kappa = 2100$ $W/m/eV^{7/2}$ is the Spitzer coefficient for classical electron thermal conductivity, $T = T_i = T_e$ is the temperature of the edge plasma at a distance s from the line of symmetry, and P_1 (W/m^3) is the heat source resulting from radial transport out from the core plasma, which is taken to be uniform in s, but decreasing exponentially with depth into the edge plasma. A second integration results in

$$T_{dp}^{7/2} + (7P_2/4\kappa)s_{dp}^2 = T_{s1}^{7/2} \quad ,$$

where T_{dp} is the temperature at $s = s_{dp}$, which is the boundary between the torus and recycle regions at the divertor plate, and T_{s1} is the temperature at the symmetry line. This leaves two parameters, T_{s1}, and T_{dp} to be determined by the boundary conditions at $s = s_{dp}$ and at $s = L$ (at the sheath).

In the recycle region, we use the one-dimensional fluid equations, and assume that $T_i = T_e = T$ and $n_1 = n_s = n$, with the dependent variables T, $p = 2enT$, and $j = neV$. The only sources and sinks considered are the particle source S, the energy sink due to ionization, and the energy source P_1. Also, we ignore the v^3 term in the energy equation, since $v << v$ (thermal) everywhere except near the sheath. The fluid equations used are:

$$dj/ds = -S, \text{ with}$$

$$S = enn_0\langle\sigma v\rangle = (p/2T)n_0\langle\sigma v\rangle \quad ,$$

$$P^2 - P_{s1}P = -(2M_i/e)j^2T \quad ,$$

$$\kappa T^{5/2}(dT/ds) + 5jT = P_1(L - s) - (\chi_i + \chi_r)j \quad ,$$

where P_{s1} is the pressure at $s = s_{s1} = 0$, and $\chi_i = -34$ eV and $\chi_r = -17$ eV are the energy costs per ionization from the binding energy and the line radiation. These three equations relate the, as yet undetermined, T_{s1} and T_{dp} to p, T, and j at $s = L$.

At the sheath where $s = L$, we require both particle and energy balance. Particle balance requires that

$$j_L = \int_{S_{dp}}^{L} S\,ds \quad ,$$

and energy balance requires that

$$Q_L = \gamma j_L T_L = P_1 L - (\chi_i + \chi_r)j_L \quad ,$$

where γ is the energy transported across the sheath per electron. Our assumptions about secondary electron emission at the plate determine the value that we choose for γ. By equating the heat transported into the sheath to Q_L, we can determine $(dT/ds)_L$, which is needed to start the numerical integration from $s = L$.

This simple approach is being used to explore the effects of the different parameters. More accurate calculations (that do not set $T_i = T_e$, for example) will be needed later.

The Vacuum Ducts

In steady state, gas particles must be removed from TIBER at the same rate that the plasma is fueled (also equal to the rate that ions leave the core plasma by radial diffusion). The fueling current is 344 A (equivalent neutral D/T), of which 18.4 A each of D and T is burned and leaves as 37 A (electrical) of He^{++}. Therefore, 45 Torr·ℓ/s of D and T molecules and 5.4 Torr·ℓ/s of He must be pumped out as gas (assuming that the gas temperature is about 500 K).

We can determine the pressure and size of the duct by equating the steady-state rate of input of particles with the total rate of gas escaping back to the plasma, plus the pumping rate of the vacuum pumps. Gas that is input into the duct comes from two sources: (1) gas from the thin layer on the plasma side of the plates conducts through the small venting ports into the duct, and (2) a fraction of the flux of fast D and T atoms that result from charge exchange are incident on the plate from the plasma side and pass through a port into the duct. This second input is significant and allows the pressure in the duct to exceed that on the plasma side of the plate. Each of the 32 pipe ducts must conduct 3.4×10^{19} molecules/s. We estimate their lengths as about 1.0 m within the neutron shielding, and expect to increase their conductances outside the shielding. Conservatively assume free molecular flow, and take the pipe conductance to be

$$C_{pipe} = (1/4)v_{mol}A_{pipe}K_{pipe} \quad ,$$

where

$$A_{pipe} = (\pi/4)\,d_{pipe}^2$$

is the cross-sectional area of the pipe, and

$$K_{pipe} = (1 + 3L_{pipe}/4d_{pipe})^{-1}$$

is the conductance relative to that of an aperture. Choose a pipe diameter d_{pipe} = 18 cm, and therefore $K_{pipe} = 0.19$, to get a pressure drop in the pipes of slightly less than 1 mTorr even in the free molecular-flow regime. In normal operation, when p_{duct}

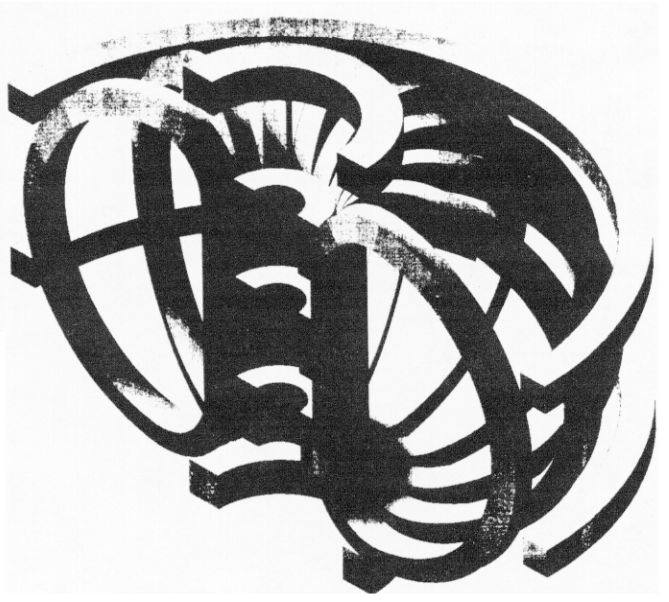

Figure 3. TIBER-II magnet set showing the internal plasma-shaping coils in place of the usual ohmic-heating coils.

= 10 mTorr, the combination of viscous plus free flow results in an even smaller pressure drop.

MAGNETS

The coil set shown in Fig. 3 for TIBER II has 15 T and 40 A/mm^2 in the winding pack of its central plasma-shaping or "pusher" coil. However, the toroidal field (TF) coils are designed to produce 12-T maximum field with the same a winding-pack current density of 40 A/mm^2. With higher fields and larger sizes than TIBER, these TIBER II coils store almost twice as much energy, about 300 MJ each for a 16 coil set. Nuclear heating to the TF coils is reduced in the TIBER-II design, but is still high by traditional standards, about 5 mW/cm^3 peak.

Two different superconductor choices have been made for TIBER II. The 15-T pusher coil will use $(NbTi)_3Sn$. This modified form of Nb_3Sn has improved performance at high fields,[3] but has poorer tolerance to irradiation by high energy neutrons[4]. As the pusher coil is essentially completely shielded by the inner sections of the TF coil set, the latter does not pose a problem. Radiation damage is a more serious concern for the TF coils. However, recent data for binary or unmodified Nb_3Sn (see Fig. 4) continue to substantiate the maintenance of the unirradiated performance beyond 10^{19} n/cm^2 at neutron energies above 0.1 MeV, (Ref. 4); consequently, this will be the superconductor of choice for the TF coils. At 12 T, 4.2 K, critical current densities upwards of 1000 A/mm^2 (exclusive of stabilizer) have been reported for Nb_3Sn. For $(NbTi)_3Sn$, critical current densities higher than 500 A/mm^2 have been reported at 15 T, 4.2 K. Table 2 (taken from a report[4] by Mauer) indicates that at 10^{10} rad epoxy insulators are degraded, but polyimides still have good compression and flexural strengths.

The benefits of improved superconductor performance are more evident in a conductor design such as the cable-in-conduit conductor design (CICC) whose constituent list is not dominated by stabilizer. The CICC design also derives benefits from the conduit as cowound structure. Variations of the CICC will be used in both the TF and poloidal field (PF) systems for TIBER II. In the PF system pusher coil, it may be necessary to grade the windings for higher current density in the lower field regions to obtain the overall pack current density goal of 40 A/mm^2; while in the TF coils, structural grading may be necessary to incorporate sufficient structure within the

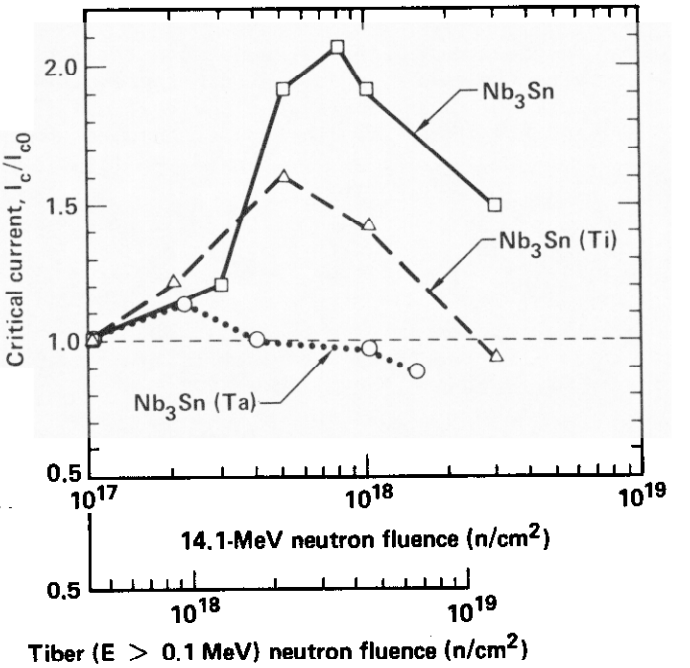

Figure 4. Critical current vs neutron fluence for modified niobium tin. The lower scale is varied to account for the energy reduction and damage potential of the neutrons reaching the magnets protected by shielding. (Data from Ref. 4.)

Table 2. Neutron irradiation data for organic insulators (irradiated to 10^8 Gy) or 10^{10} rad).

Material	Unirradiated strength		Irradiated strength	
	Compression (MPa)	Flexure	Compression (MPa)	Flexure
G-10	886	1100	65	95
G-10 BF		990		108
G-11	826	1113	62	110
Epikote 828 (epoxy)	513	165	125	25
Stycast 2850 (epoxy)	570	262	50	57
Spaulrad (polyimide)	680	990	400	640
Norplex (polyimide)	900	690	900	445
Vespal (polyimide)	250	320	255	320

low field windings to support the centering loads in the central, straight-leg portions of these coils. For example the high field TF conductor can have a uniform jacket as in Fig. 5(a), whereas the low field-conductor would have a more crush resistant jacket as in Fig. 5(b).

STRESS ANALYSIS

We created a finite element model, which contains the center post (1-m diameter), the support and pusher coils, and the vertical legs of the TF coils. This model assumes that pins between the TF coil legs successfully transmit the overturning forces shown in Fig. 6 to the outer skin of the coil case. The model in Fig. 7 with exaggerated deflections gives 575-MPa (effective) stress in the outer skin. Both centering and overturning forces were present. When only the overturning force was present, the outer skin stress was slightly lower.

An analytic calculation was also performed that included two assumptions: (1) the center post contributes nothing to resist the turnover torque, and (2) the outer and inner skins of the TF coil rotate at the same angle again. This was in good agreement with the Gemini finite element calculation.

NUCLEONICS

The principal nuclear design objective for TIBER II is providing the TF superconducting (SC) coils with the shielding required for a machine lifetime of 10^8 burn seconds, while minimizing impact on machine size and costs.

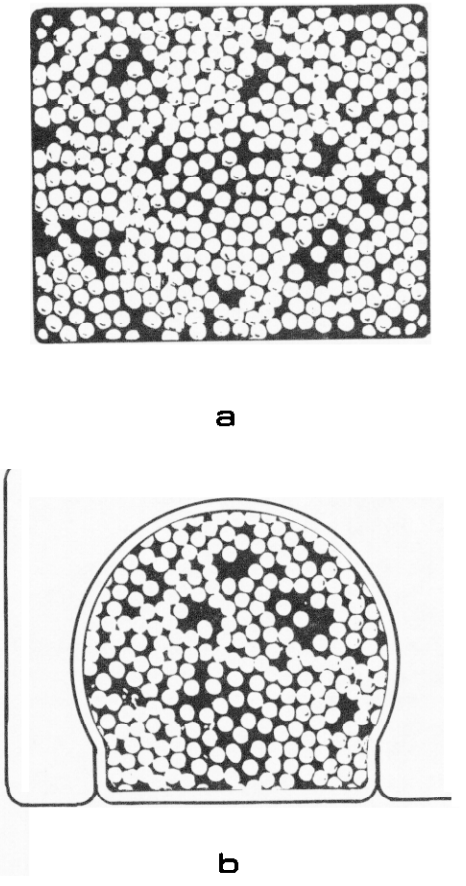

Figure 5. (a) A cable in conduit conductor (CICC) with a uniform steel jacket. (b) The jacket is concentrated on one side to be more resistive to bearing loads from hydrostatic forces on the inner leg of the TF coil.

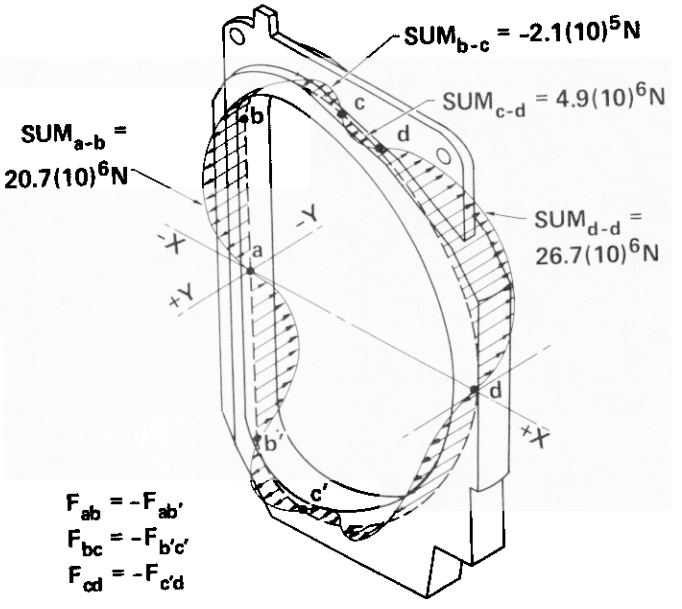

Figure 6. TIBER-II TF-coil magnetic force (Y or azimuthal component only).

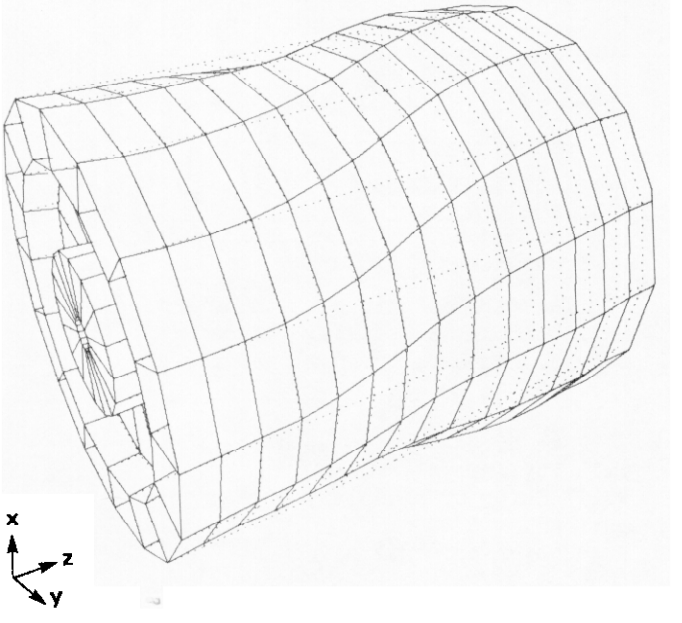

Figure 7. Exaggerated deflections of the inner leg of the TF coil produces 575-MPa stresses.

Initial scoping studies of an earlier, slightly smaller version of TIBER indicate that TIBER II, as presently configured, can reach the 10^8 s goal without exceeding heating and radiation damage limits of 10^{19} n/cm^2 (E > 0.1 MeV) in Nb_3Sn and 10^{10} rads in polyimide in the critical inboard leg of the TF coil (Refs. 1 and 5). Peak and total heating in the TF, SC coils is expected to be no more than 10 mW/cm^3 and 50 kW, respectively. The effects of possible beam lines and other penetrations have yet to be addressed. At a fusion power of 277 MW, the first wall-loading peaks on the midplane on the outer leg at 1.8 MW/m^2, and on the inner leg at 1.3 MW/m^2, while the average wall loading is 1.2 MW/m^2 as shown in Fig. 8 (Ref. 6). In addition to shielding, we will also be assessing the prospects and costs for breeding tritium in TIBER II. Tritium availability or cost from external sources will dictate if T breeding is required or is cost effective. We are considering a number of low-technology blanket options with low-pressure water-cooled Be/LiAl/Al and Be/H_2O + LiX/SS blankets as top contenders.

OPERATION AND TESTING

To facilitate a definition of TIBER II, Table 3 represents a simplified operating schedule. After a checkout Phase I, we expect a decreased availability of only ~10% in Phase II because of activation for initial verification and operating tests of the system under DT operation. The final Phase III availability is set at 30%, as determined by fluence requirements (see below).

An important question is whether the engineering test reactor (ETR) should attempt high end-of-life fluences. We can delineate

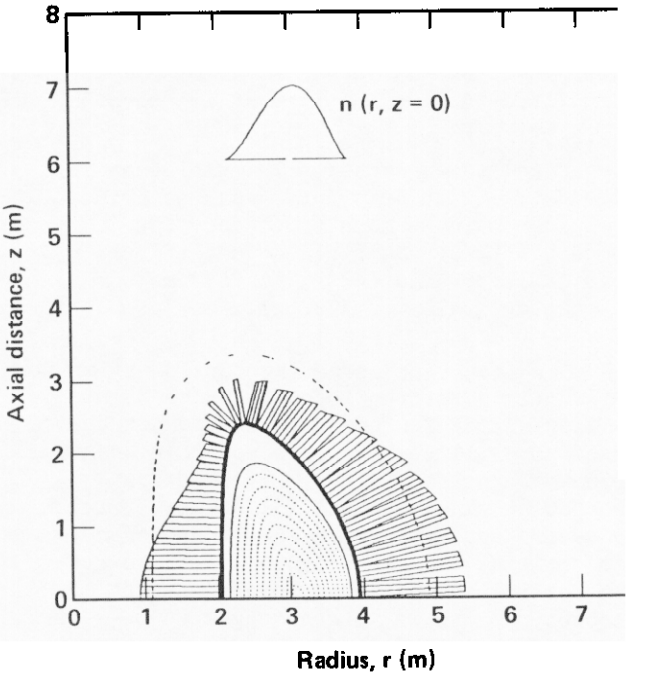

Figure 8. Wall-loading distribution in TIBER-II.

Table 3. Projected TIBER-II operation schedule.

Phase (y)	Duration (y)	Emphasis	Availability (%)	Annual T_2 consumption (kg/y)	Integrated 14-MeV fluence peak/av ($MW \cdot y/m^2$)
Phase I (1998-1999)	1	H_2 checkout	15	--	--
Phase II (1999-2001)	2	DT operation verification	10	1.60	0.36/0.24
Phase II (2001-2011)	10	Engineering testing	30	4.78	5.40/3.6

the following three approximate operating times (OT) for fluence: (1) short-term requirements for blanket and component operation:

$$0.07 \leq OT \leq 0.2 \text{ MW y/m}^2;$$

(2) intermediate requirements for component reliability, verification and end-of-life in the more sensitive components (e.g., insulators, limiter surfaces):

$$0.2 \leq OT \leq 3 \text{ MW y/m}^2;$$

(3) long-term fluence for structural material testing:

$$OT > 3 \text{ MW y/m}^2.$$

A high fluence makes possible the characterization of component reliability and material damage with a greater credibility. However, a high fluence also requires a high average availability, which may preclude the deployment of subsequent advanced concept facilities during the life of the machine. We believe that a fluence goal of ~3 MW y/m^2 (average) is warranted. The employment of steady-state current drive as a baseline requirement does much to enhance the credibility of the fluence goal through high availability. Table 4 lists our major operating goals for TIBER-II.

One important operating consideration for TIBER-II is tritium supply. Three main reasons exist for breeding tritium in the machine: (1) to make up a possible shortfall from external suppliers, (2) to offset operating expenses, and (3) to test tritium breeding and extraction under reactor-relevant conditions. The last of these points refers to testing of reactor-relevant blanket prototypes and is not envisaged to be a part of the baseload tritium breeding system, which will likely comprise reliable, low-temperature, low-technology modules. We note from Table 3 a requirement for ~4.8 kg of tritium per year in the final operating phase. At the current U.S. commercial price of 10M$/kg, purchase of all tritium requirements from an external source would result in an annual tritium cost of ~50M$/y. It appears there would be sufficient tritium inventories in Canada, the U.S. or the U.S.S.R. to supply the yearly requirements. Accordingly, the fraction of the machine devoted to baseload breeding will result from a cost-benefit analysis including operating cost offsets, testing space requirements, and external supply uncertainties.

Table 4. Major operating goals for TIBER-II.

1. Testing of blankets, tritium-production, plasma-engineering components and advanced reactor concepts in a reactor-relevant environment.
2. Testing of factors which determine reliability, maintainability, availability, safety, and environmental aspects of a fusion reactor.
3. Steady-state burn with equilibrium impurity removal.
4. Testing of a variety of current-drive options.
5. Use of poloidal divertors for impurity control.
6. Flux requirements: $\langle r \rangle \geq 1$ MW/m^2.[a]
7. Fluence requirements: $\langle OT \rangle \geq 3$ $MW \cdot y/m^2$.[a]
8. Full-power lifetime $\geq 10^8$ burn·s.
9. Final-phase availability $\geq 30\%$.
10. Final-phase operating life ≤ 10 y.

[a] Peak values will be ~1.5 higher than this.

ACKNOWLEDGMENT

This work was performed under the auspices of the U.S. Department of Energy by the Lawrence Livermore National Laboratory under contract number W-7405-ENG-48.

REFERENCES

1. C. D. HENNING, B. G. LOGAN et al., TIBER-Tokamak Ignition/Burn Experimental Research Final Design Report, Lawrence Livermore National Laboratory, Livermore, CA, UCID-20589 (1985).

2. C. F. F. KARNEY and N. J. FISCH, Phys. Fluids 28, 116 (1985).

3. M. SUENAGA, "Workshop on Conductor-Sheath Issues for ICCS," Brookhaven National Laboratory, Upton, NY, July 1985.

4. R. FLUKIGER, W. MAURER, F. WEISS, P. A. HAHN, and M. W. GUINAN, private communication (1986).

5. W. MAURER, Neutron and Gamma Irradiation Effects on Organic Insulating Materials for Fusion Magnets, Kernforschungszentrum Karlsruhe Report, KFK 3974 (1985).

6. NEWLIT-A General Code for Neutron Wall Loading Distribution in Toroidal Reactors, Fusion Technol. 8 (1), Part 2A, 608 (1985); calculation done by M. Sawan from University of Wisconsin--Madison.